GSICS Global Space-based Inter-Calibration System

Quarterly

Newsletter–Fall 2016 Issue

Volume 10 Number 3
2016
doi: 10.7289/V5PC30DM

Manik Bali, Editor

In This Issue


Sentinel-3A: Curtsey ESA

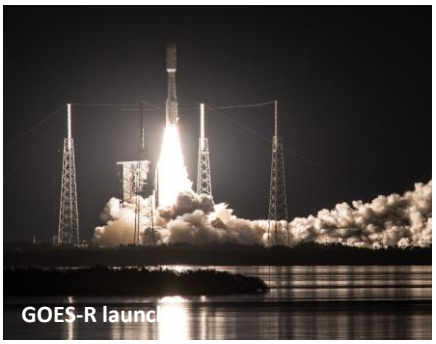
GOES-R launc

Initial comparison between Sentinel-3A SLSTR and IASI aboard MetOp-A and MetOp-B

by Igor Tomazic, Anne O'Carroll, Tim Hewison, Jörg Ackerman,(EUMETSAT), Craig Donlon, Jens Nieke, Bouwe Andela,(ESA/ESTEC), Dorothee Coppens (EUMETSAT), Dave Smith (RAL)

The Copernicus Sentinel-3A satellite was successfully launched on 16th February 2016. Commissioning and operational activities have been progressing with the In-Orbit Commissioning Review completed in July 2016 and public release of level 1 data in Q4 2016.

Aboard the Sentinel-3A satellite is a dual view Sea and Land Surface Temperature Radiometer (SLSTR) implemented to fulfil requirements of delivering accurate reference surface ocean, land and ice temperature and to maintain continuity with AATSR series of instruments (Donlon et al., 2012). To examine the accuracy and continuity we performed preliminary comparisons of Sentinel-3A SLSTR against MetOp-A and MetOp-B Infrared Atmospheric Sounding Interferometer (IASI) measurements, using simultaneous nadir overpasses (SNOs) and following the inter-comparison already performed between AATSR and IASI-A (Bali et al., 2016, Illingworth et al., 2009). IASI hyperspectral radiances were convolved with Sentinel-3A SLSTR spectral response functions (SRF) of bands S8 and S9 (10.8 µm and 12 µm), in order to derive IASI simulated SLSTR S8 and S9 brightness temperatures (BT).

These convolved IASI observations were collocated (in space and time) with SLSTR L1 S8 and S9 BT nadir view measurements which were averaged over the IASI FOV (estimated as an ellipse).

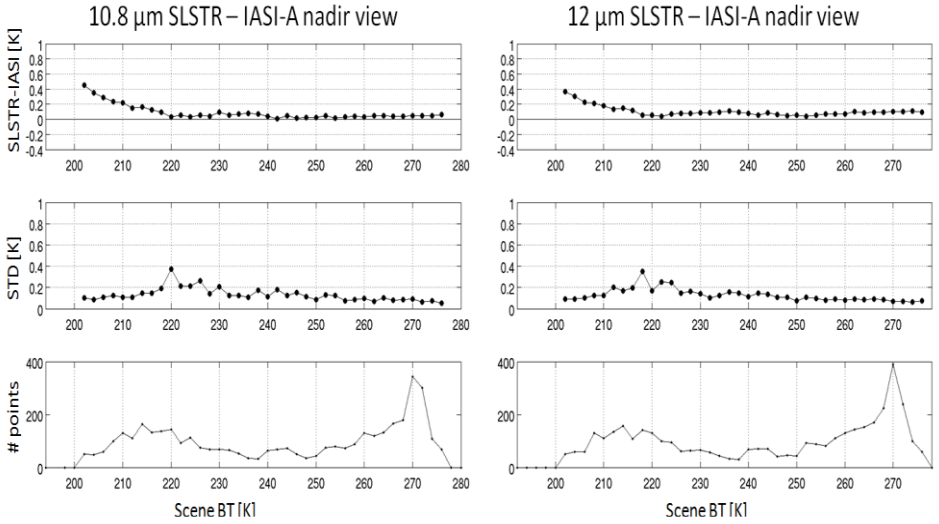

Figure 1. Scene temperature dependence of homogenous SLSTR-A and IASI-A differences for nadir view BT channel 10.8 µm (S8) (left panel) and BT channel 12 µm (S9) (right panel).Upper panels show averaged values over 2 K bins, middle panels show corresponding standard deviations and the bottom panels show number of points for each bin.

Crossovers were detected using orbital modelling with maximum absolute time differences of 5 min and a maximum distance of 10 km between the satellite ground tracks. Using these spatio-temporal constraints, each crossover event lasted for 2 days, having around 50 crossovers concentrated over the south and north polar regions. Crossover events occurred approximately every 17 days. For this initial analysis we analyzed five crossover events between April and August 2016. We applied standard Global Space-based Inter-Calibration System (GSICS) collocation criteria (Hewison et al, 2013): the same criteria that was used to produce pixel matchups (5 minutes time difference between central SLSTR and IASI observations) with additional constraints on the incidence angles such that their atmospheric path difference is less than 1% (i.e. $|\Delta\sec(\vartheta)/\sec(\vartheta)| < 0.01$). Additionally, we performed analysis on homogenous IASI pixels identified through the standard deviation of SLSTR pixels aggregated over the IASI IFOV being below or equal 0.4 K. Initial results suggest very good (below 0.1 K on average) correspondence of SLSTR-A both with IASI-A and IASI-B. The differences between homogenous SLSTR-A and IASI-A collocations as a function of scene temperature shows very small and almost constant bias ($\leq$0.1 K) for the temperature range between 220 K to ~280 K. For very low scene temperatures, between ~200 K and 220 K, scene temperature dependence was observed with an increase in the SLSTR-A – IASI-A (and IASI-B) average bias of up to 0.4 K, which is still within uncertainty of IASI absolute calibration for cold scenes. Finally, higher biases for scene temperatures around and below 200 K (more pronounced in channel S8) require further analysis since the values potentially include unflagged erroneous data close to the lower boundary of dynamic range. It should be noted that higher bias in the cold temperature range is impacting overall statistics therefore with improved flagging erroneous data we are expecting further improvements in the overall statistical results. Applying double difference method between SLSTR-A – IASI-A and SLSTR-A – IASI-B (Figure 2) over homogenous collocations we observe similar trend as for IASI-A with a higher differences towards cold scene temperatures. Similar double difference analysis using MSG SEVIRI show a pronounced trend, with IASI-B being slightly colder than IASI-A towards colder temperatures. Since the SNO crossovers are located only over the polar regions, the SNO methodology

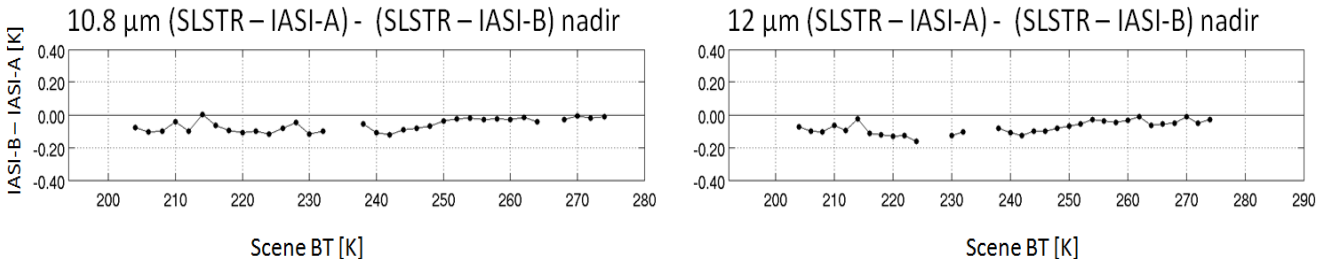

Figure 2. Double differences between SLSTR-A - IASI-A and SLSTR-A - IASI-B over homogenous collocations for S8 channel 10.8 µm (left) and S9 channel 12 µm (right). Small negative bias of IASI-B compared to IASI-A exists for both channels (S8: -0.06±0.04 K and S9:-0.08±0.04 K).

Return to Page 1

covers scene temperatures mostly below ~280 K for specified channels. To perform a verification with warmer scene temperatures (>280 K) over low-latitude regions requires a different approach, using a quasi SNO (QSNO) analysis with relaxed time differences criteria (of up to 20 min). The methodology was implemented and tested on several crossovers, and to produce more tangible results it requires processing of several months of data using a nominal cloud mask and with improved geo-location accuracy.

Future work will also include assessment of the oblique view, gap filling of IASI spectra for SLSTR band 7 (3.7 µm) and implementation of all variables and flags to perform monitoring in a quasi-operational manner.

This preliminary result shows similar results as obtained with AATSR-IASI inter-comparison (Illingworth et al., 2009) and promise for delivering high accuracy SLSTR surface temperatures and maintaining continuity of AATSR instruments.

SLSTR Level-1B data are publicly available from 17th November 2016 through EUMETSAT Data Centre and Copernicus Online Data Access. (http://www.eumetsat.int/website/home/Data/CopernicusServices/Sentinel3Services/index.html)

References

Donlon, C., et al. 2012. "The Global Monitoring for Environment and Security (GMES) Sentinel-3 Mission." *The Sentinel Missions - New Opportunities for Science* 120 (May): 37–57. doi:10.1016/j.rse.2011.07.024

Hewison T. et al (2016), Prime GSICS Corrections, using double-differences of IASI-A and -B against the IR channels of Meteosat/SEVIRI, Poster presented at IASI Conference, Antibes Juan-les-Pins, France, 11 April 2016.

Illingworth, S. M., J. J. Remedios, and R. J. Parker. 2009. "Intercomparison of Integrated IASI and AATSR Calibrated Radiances at 11 and 12 μm." *Atmospheric Chemistry and Physics* 9 (18): 6677–6683. doi:10.5194/acp-9-6677-2009

Discuss the Article

Update of the absolute calibration parameters of FASat-Charlie using RapidEye

by Carolina Barrientos (Aerial Photogrammetric Service of Chilean Air Force (SAF- FACH)), Cristian Mattar (Laboratory for Analysis of the Biosphere (LAB) of University of Chile), Theodoros Nakos (Crux Technologies) and Waldo Perez (OTERRA, Major University).

Radiometric calibration parameters were updated for multispectral bands of the sensor on board of the FASat-Charlie mission (Mattar *et al*., 2014) using RapidEye (RE4) imagery acquired over the Frenchman Flat calibration site. The simultaneous nadir overpass (SNO) approach, was applied following Teillet *et al*. (2006), and allowed for the compensation of in-orbit variations of the radiometric response of the Chilean satellite.

Calibration Method

In the absence of on-board radiometric calibration sources, a well-known reference instrument is an alternative to update the absolute response of a sensor. In the case of RapidEye, the absolute radiometric calibration parameters of all the Multispectral Imager (MSI) of the constellation are monitored and updated relying on vicarious methods (Brunn *et al*., 2010). The main advantage of such calibration approaches is they do not introduce additional biases generated by degradation of the OBC sources.

The simultaneous nadir acquisitions for the cross-calibration of FASat-Charlie were performed by both satellites on 25 July 2014 (Barrientos *et al*., 2016). The Getis-Ord statistic (*Gi*) (Getis and Ord, 1992), Moran's *Index (I)* (Anselin, 1995), coefficient of variation (CV) and average TOA reflectance values were employed to select the most homogeneous and reflective areas across the calibration site.

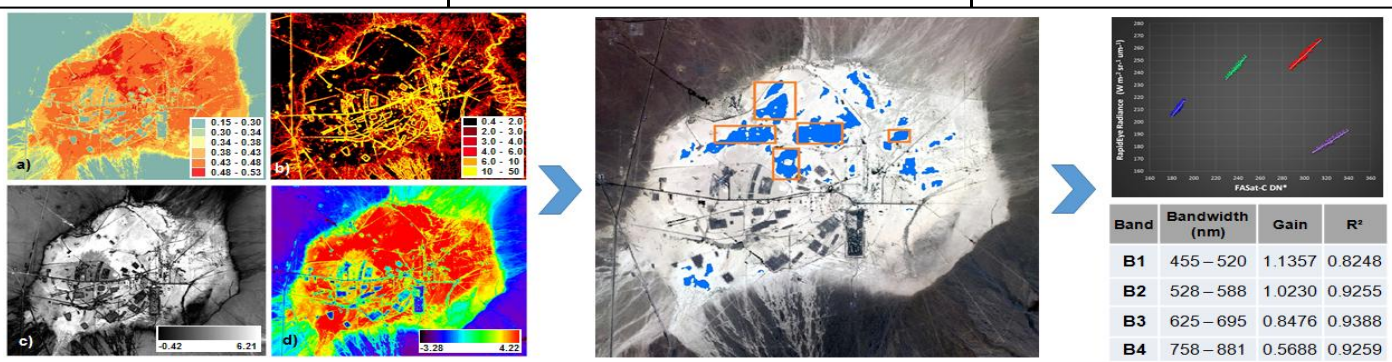

Band	Bandwidth (nm)	Gain	R^2
B1	455 – 520	1.1357	0.8248
B2	528 – 588	1.0230	0.9255
B3	625 – 695	0.8476	0.9388
B4	758 – 881	0.5688	0.9259

Figure 1. Average TOA reflectance (a), CV % (b), Moran Index (c) and Getis Ord indicator (d) were used to define the cross-calibration areas (blue regions), leading to the estimation of a new set of calibration parameters for FASat-Charlie.

Band	Calib.	Bias Errors (W m^{-2} sr^{-1} µm^{-1})						Absolute Errors (%)							
		MBE	St Dv	Median	Max	Min		RMSE	MAPE	St Dv	Min	1st Quart	Median	3rd Quart	Max
B1	Pre-flight	9.03	2.43	9.26	16.48	4.70		6.27%	6.01%	1.81%	3.03%	4.80%	5.53%	7.35%	13.36%
	Cross-cal	0.17	2.79	-0.29	8.11	-5.45		1.94%	1.51%	1.23%	0.00%	0.56%	1.20%	2.15%	8.12%
B2	Pre-flight	7.57	3.22	8.06	17.10	1.12		5.00%	4.61%	1.93%	0.79%	3.29%	4.26%	5.88%	13.10%
	Cross-cal	1.67	2.82	1.33	8.95	-5.48		2.28%	1.71%	1.52%	0.01%	0.53%	1.23%	2.53%	9.90%
B3	Pre-flight	8.17	2.22	7.91	14.73	2.45		5.18%	4.93%	1.59%	1.40%	3.90%	4.86%	5.79%	9.98%
	Cross-cal	3.36	2.27	3.51	9.80	-3.30		2.75%	2.31%	1.50%	0.00%	1.20%	2.14%	3.09%	7.40%
B4	Pre-flight	-10.4	5.28	-8.02	-0.23	-22.76		7.80%	7.52%	2.08%	0.24%	5.97%	7.50%	9.25%	12.66%
	Cross-cal	4.0	1.75	3.62	9.41	-2.88		3.56%	3.05%	1.84%	0.00%	1.53%	3.04%	4.43%	9.60%

Table 1. Results of the validation sample. Pre-flight and updated gains were used to calculate FASat-Charlie TOA radiances and then compared with RapidEye.

The following threshold values were considered to identify regions with the characteristics of the former LSpec site:

CV $\leq$ 2%, $Gi \geq 3.2$, $I \geq 3.5$ and $\rho \geq 0.3$.

The cross-calibration samples (130) were extracted from both images, within the resulting clusters (Figure 1). Seven scans from the EO-1 Hyperion sensor were employed to calculate the Spectral Band Adjustment Factor (SBAF) (Chander *et al.*, 2013), and to compensate the differences between the FASat-Charlie and RapidEye bands. Samples for SBAF calculation were extracted from the homogeneous and reflective clusters.

The resulting SBAFs values (one per band) were applied to the digital numbers (DN) of FASat-Charlie. Then, linear adjustments were performed to update the gains of the multispectral bands. A validation process was conducted over the whole common coverage area; and 300 samples were collected over targets with different spectral behavior (*e.g.* low reflective soils and vegetation). At-sensor radiances of these samples were calculated using both gain sets. However, considering the reduced extension of the dark areas (few pixels) and the ground sampling distance of Hyperion, approximated SBAFs values were calculated for the compensation of such validation surfaces.

Radiometric Cross-Calibration Result

The adjusted FASat-Charlie radiances of every sample were compared with the respective RapidEye values, calculating biases and absolute percentage difference values. After that, the main summary statistics such as Root Mean Square Error (RMSE), Mean Bias Error (MBE) and Mean Absolute Percentage Error (MAPE) were obtained. Results showed an improvement in the accuracy of at-sensor radiances of FASat-Charlie and a reduction of biases and absolute errors (Figure 2 and Table 1).

Conclusion and Future Activities

Our results show the importance of using data collected over an endorsed site to cross-calibrate a satellite sensor.

This procedure will allow the direct comparison and full integration of information obtained by different missions, hence cross-calibration efforts against RapidEye will continue. Recently, a vicarious calibration campaign was performed in "El Tambillo", Atacama Desert, Chile (Pinto *et al.*, 2015). During this campaign, ground reflectance measurements were conducted on a very homogeneous surface and acquisitions of RapidEye and FASat-Charlie are available.

Then, the application of the reflectance–based vicarious calibration method will be considered, along with cross-calibration as an additional validation tool. Moreover, other sites are being explored for the same purpose, such as pseudo-invariant calibration sites (PICS) and other areas of the world with heterogeneous land covers.

Return to Page 1

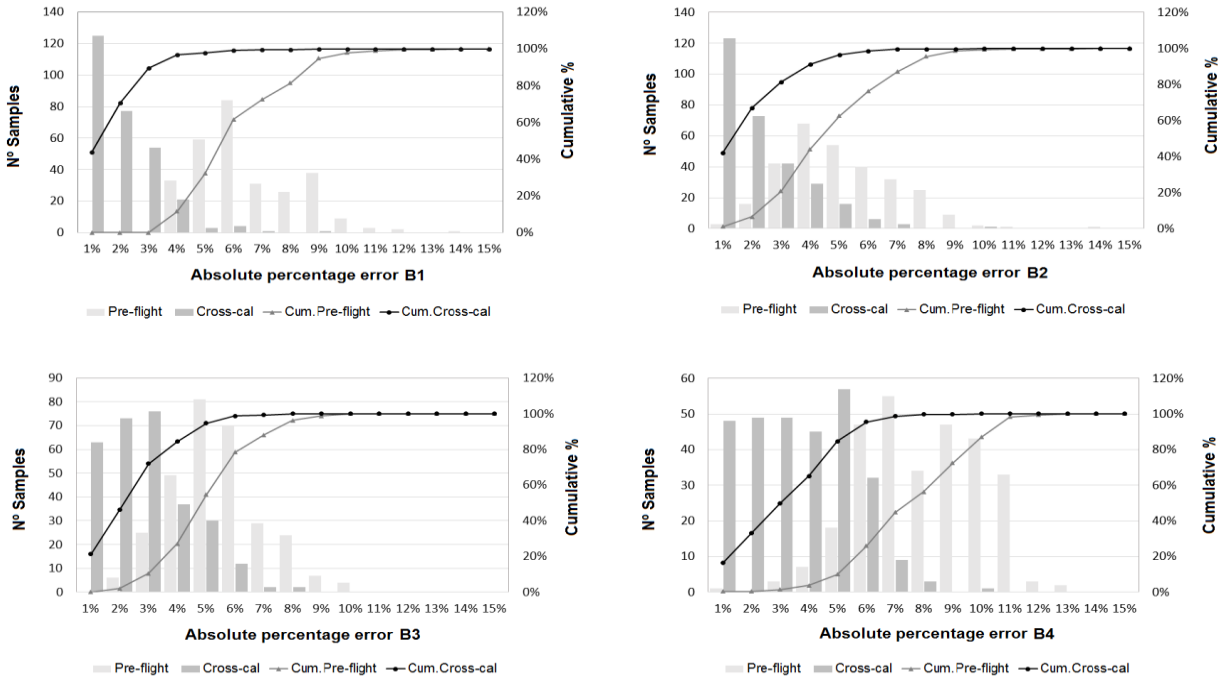

Figure 2. Histograms of absolute percentage errors for FASat–Charlie evaluation samples. Results derived using pre-flight and updated gains are shown in light and dark gray, respectively.

Acknowledgements

This work was supported by the Aerial Photogrammetric Service (SAF) and the Space Operations Group (GOE) of the Chilean Air Force (FACH). RapidEye data were provided by Blackbridge.

References

Mattar, C.; Hernández, J.; Santamaría-Artigas, A.; Durán-Alarcón, C.; Olivera, L.; Inzunza, M.; Tapia, D.; Escobar-Lavín, E. A first in-flight absolute calibration of the Chilean Earth Observation Satellite. *ISPRS J. Photogramm. Remote Sens*. 2014, 92, 16–25. DOI: 10.1016/j.isprsjprs.2014.02.017

Teillet, P.M.; Markham, B.L.; Irish, R. R. Landsat Cross–Calibration based on near simultaneous imaging of common ground targets. Remote Sens. Environ. 2006, 102, 264–270. DOI:10.1016/j.rse.2006.02.005

Brunn, A.; Naughton, D.; Weichelt, H.; Douglass, S., Thiele, M.; Oxfort, M.; Beckett, K. The Calibration Procedure of the Multispectral Imaging Instruments on Board the RapidEye Remote Sensing Satellites. International Calibration and Orientation Workshop, EuroCow, Castelldefels, Spain, 2010.

Getis, A.; Ord, J.K. The Analysis of Spatial Association by Use of Distance Statistics. *Geogra. Anal*. 1992, 24, 189–206. DOI: 10.1111/j.1538-4632.1992.tb00261.x

Anselin, L. Local Indicators of Spatial Association – LISA. *Geogra. Anal*. 1995, 27, 93–115.DOI: 10.1111/j.1538-4632.1995.tb00338.x

Chander, G.; Mishra, N.; Helder, D.; Aaron, D.; Angal, A.; Choi, T.; Xiong, X.; Doelling, D. Applications of Spectral Band Adjustment Factors (SBAF) for Cross–Calibration. *IEEE Trans. Geosci. Remote Sens*. 2013, 51, 1267–1281; DOI: 10.1109/TGRS.2012.2228007

Barrientos, C.; Mattar, C.; Nakos, T.; Perez, W. Radiometric Cross-Calibration of the Chilean Satellite FASat-C Using RapidEye and EO-1 Hyperion Data and a Simultaneous Nadir Overpass Approach. *Remote Sens.*2016, *8*, 612. DOI:10.3390/rs8070612

Pinto, C.T; Ponzoni, F.J.; Barrientos, C.; Mattar, C.; Santamaría-Artigas, A.; Castro, R.M. Spectral and atmospheric characterization of a surface at Atacama Desert for earth observation sensors calibration. IEEE Geosci. Remote Sens. Lett. 2015, 12, 2227–2231. DOI: 0.1109/LGRS.2015.2460454

Discuss the Article

doi: 10.7289/V5PC30DM
GSICS Quarterly: Fall Issue 2016 Volume 10, No. 3, 2016

Inter-calibration of Belarusian Satellite with other imagers

by Volha Siliuk and Leonid Katkovsky (Scientific Research Institute of Applied Physical Problems of Belarussian State University)

For extraction of information about the Earth surface from satellite data, it is necessary to periodical check a satellite sensor's stability. Cross-calibration of two or more sensors is one of the ways to perform such checks.

The Belarusian Satellite (BS) was launched in 2012. BS regularly takes pictures of the Earth surface, and these data are used for solving different problems. Cross-calibration of the data from the BS sensor and from other concurrent satellite sensors such as Landsat 8, EO-1 (ALI & Hyperion) and AVIRIS (airborne) was performed [1]. The technique for the cross-calibration is described below.

Cross-calibration technique for multispectral sensors with similar spectral bands.

Satellite images contain the data in units of digital numbers (DN) that belong to specific range for each sensor. To compare the data from different sensors, it's necessary to convert DN into spectral radiance units (W/(nm*m^2*sr)). For this, the following linear equation is generally used:

$$B = c_1 DN + c_0 \quad \ldots \qquad (1)$$

where c_1 and c_0 are calibration coefficients. There is one pair of calibration coefficients for each band of a sensor. At the first step of cross-calibration the DN's of each pixel of the image are converted into effective radiance values for each band.
The effective spectral radiance that satellite sensors measure in a band can be defined as

$$B = \int_{\lambda_1}^{\lambda_2} S(\lambda) B(\lambda) d\lambda \Big/ \int_{\lambda_1}^{\lambda_2} S(\lambda)\, d\lambda \quad \ldots (2)$$

Where $S(\lambda)$ is the spectral sensitivity function of the band, $B(\lambda)$ is the spectral radiance on the top of atmosphere (TOA), and λ_1 and λ_2 are the boundary wavelengths for a certain spectral band.

To improve the comparison accuracy of two sensors, it is necessary to take into account the differences in spectral sensitivity of the bands, and the spectral bands' location and bandwidth. These differences are shown in Figure 1, where spectral sensitivities of comparable bands of BS, Landsat8 and EO-1 are illustrated.

As we see from (2), the effective radiance depends not only on band spectral sensitivity, but also on the TOA spectral radiance. As we do not know the radiation spectra of the surface during quasi-synchronous measurements, a response (effective radiance) of typical spectra for the underlying surface was calculated by (2) for each band to account for differences in response to a particular spectrum due to the differences in sensitivity.

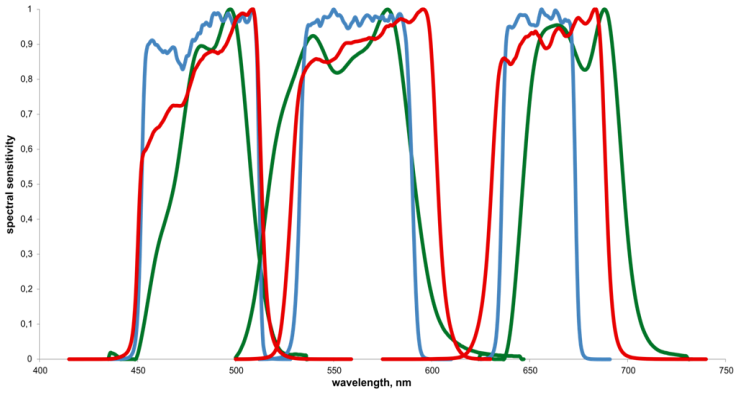

Figure 1. Relative spectral sensitivities of BS (green lines), Landsat 8 (blue lines) and EO-1 ALI (red lines).

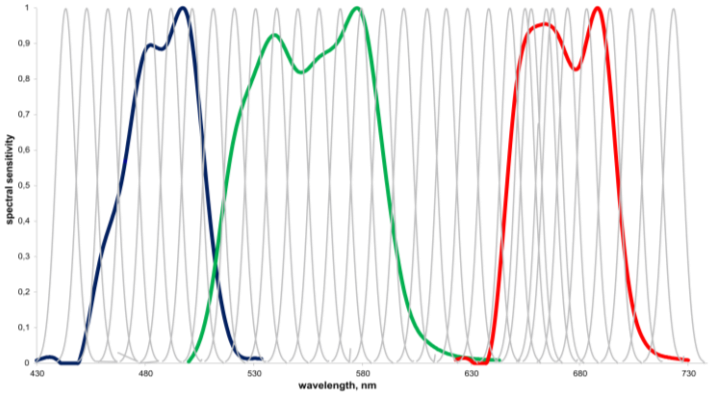

Figure 2. Relative spectral sensitivities of BS bands and bands 9-40 of AVIRIS.

Return to Page 1

The user determines the type of the surface by the image or a map. Spectra measured by PSS (Photospectral system, development by Scientific Research Institute of Applied Physical Problems BSU) from the International Space Station were used as $B(\lambda)$ in this research. The ratio of the responses for the pair of bands (3) uses as a correction factor, k, in process of comparison the data from two satellites.

$k_1 = B_{sat1}/B_{sat2}$ ….(3)

Besides the differences in observing conditions that were taken into account, another factor was added for increased accuracy. The radiances satellite sensors measure depend on the solar zenith angles ($\theta_{sat1}, \theta_{sat2}$) that are different when the two sensors observe the same surface due to differences in observation times.

In this case, a correction factor can be calculated as:

$k_2 = E_{sat1}/E_{sat2} = \cos\theta_{sat1}/\cos\theta_{sat2}$ ..(4)

where E_{sat1} and E_{sat2} are irradiances corresponding to the observing time for each satellite.

For comparison of measurements, the same almost homogeneous Earth sites are selected within overlapping spatial regions recorded by both sensor. Taking into account the different spatial resolution and image orientation of two sensors, the spatial averaging measured radiances by each sensor was carried out within approximately the same spatial regions of interest.

The correction factors previously calculated were applied to obtain the desired ratio of effective radiances measured by different sensors.

Cross-calibration technique for multispectral and hyperspectral sensors

Cross-calibration techniques for multispectral and hyperspectral sensors have some other features. To convert DN values for hyperspectral sensors such as AVIRIS and Hyperion into radiances only a single gain coefficient is used.

In addition, when cross-calibrating the BS sensor with a hyperspectral imaging systems, it is necessary to calculate the average value of the effective radiances on a number of adjacent bands for the hyperspectral sensor to cover each wide BS sensor band (figure 2). In this case, it's necessary to sum up the contributions of the hyperspectral sensor bands, corresponding to a combined width for each of the three multispectral BS bands. The following equation is used:

$$B_j = k_{1j} \sum_{i=n_{j1}}^{n_{j2}} B_i^{hyp} \Big/ \left(n_{j2} - n_{j1}\right) \cdots (5)$$

where B_j is an averaged value within the bands of hyperspectral data radiance, n_{j1} and n_{j2} are the number of the first and the last hyperspectral bands, which corresponds to j-band of BS, j=1,2,3 – correspond to band 1, band 2, band 3 of BS; B_i^{hyp} is the measured radiance in band i of the hyperspectral sensor.

The first correction factor is calculated by a formula similar to (2):

$$k_{1j} = \bar{B}_j^{БКА} \left[\sum_{i=n_{j1}}^{n_{j2}} \bar{B}_i^{hyp} \Big/ \left(n_{j2} - n_{j1}\right) \right]^{-1} \cdot\cdot \quad (6)$$

where $\bar{B}_j^{БКА}$ and $\bar{B}_i^{hyp}$ are effective radiances of band j of the BS and band i of the hyperspectral sensor, respectively, calculated by using the same typical spectrum of underlying surface at the TOA.

Results

Information about the data that were compared and results of cross-calibration are shown in Table 1. It contains absolute ratio errors calculated

Place, date and observation time	Type of underlying surface	Δ, %		
		B	G	R
Belarussian satellite vs Landsat 8				
Libya, 12.09.2013 BS: 10:10:56 L8: 9:16:06	Desert	5	5	2
Russia (Nizhny Novgorod region), 18.04.2014 BS: 8:03:57 L8: 8:04:15	Forest	10	5	3
	Field	11	9	14
Russia (St. Petersburg region), 18.11.2014 BS: 8:54:04 L8: 9:05:32	Field	15	5	15
	Forest	13	-2	10
Kamchatka Peninsula, 09.06.2015 BS: 00:29:50 L8: 00:32:24	Snow	17	18	20
Island Novaya Zemlya, 02.08.2015 BS: 5:07:42 L8: 08:04:10	Snow	3	3	6
Belarussian satellite vs EO-1 ALI				
Arabian Peninsula, 25.10.2014 BS: 9:05:00 EO-1: 7:06:41	Desert	-2	-7	-13
Arabian Peninsula, 24.07.2015 BS: 9:10:00 EO-1: 6:31:25	Desert	-3	-6	-3
Belarussian satellite vs EO-1 Hyperion				
Arabian Peninsula, 25.10.2014 BS: 9:05:00 EO-1: 7:06:41	Desert	-11	-6	-9
Belarussian satellite vs AVIRIS				
California, USA, 25.11.2013 BS: 19:12:16 AVIRIS: 20:50:00	Mountains	-2	15	14
		-1	10	12
	Field	-13	-12	-7

Table 1: The results of cross-calibration calculations for nine selected sites.

as:

$$\Delta = \left(1 - \frac{B_{BS}}{B_{LS8,EO-1,AVIRIS}}\right) * 100 \quad ....(7)$$

Thus, as the result of performed cross-calibration, we can conclude that BS data are reliable enough because derived different sensors ratios of radiances measured quasi-synchronously above the same underlying surface are within the total uncertainties, determined by accuracy of absolute sensors calibrations. Calibration uncertainty of the BS, Landsat 8, EO-1 and AVIRIS sensors is no more than 5% [2-5]. The reasons for the larger biases are under investigation.

Analysis of images received during the last few years by BS did not reveal any tendency to changes in the BS sensor sensitivity, and this means it is stable and additional calibrations adjustments are not currently required.

References

1. Siliuk, O., Katkovskii, L., 2016, Methods and results of image cross-calibration of the Belarusian satellite and other sensors. Current problems in remote sensing of the earth from space, Vol. 13, No 4, 261-270, DOI: 10.21046/2070-7401-2016-13-4-261-270

2. Belyaev, Y., et al., 2012, Spectral brightness passing schemes and methods of high-resolution and large aperture equipment calibration. The 10th all-Russia Open Conference "Current Problems in Remote Sensing of the Earth from Space", Book of Abstracts.

3. Markham, B., et al., 2014, Landsat-8 Operational Land Imager Radiometric Calibration and Stability. Remote Sensing, Vol. 6, Issue 12, 12275-12308, DOI:10.3390/rs61212275

4. Mendenhall, J., Lencioni, D., Evans J., 2005, Spectral and Radiometric Calibration of the Advanced Land Imager. Lincoln Laboratory Journal, Vol. 15, No. 2, 207-224.

5. Chrien, T., et al., 2000, Calibration Validation of the AVIRIS Portable Radiance Standard. AVIRIS Workshop Proceeding

Discuss the Article

Variability in Inter-Sensor Biases within the GPM Constellation

by John Xun Yang, CICS/UMD

Spaceborne microwave radiometry observes the earth-atmosphere system in near all-weather conditions and plays a major role in weather and climate science and associated applications. Inter-calibrating different radiometers has become an indispensable task for diagnosing instrument performance and integrating the microwave satellite constellation data. Because inter-calibration affects both base radiance data and downstream science products, it is critical to examine inter-sensor performance before recalibration.

In this study, we have investigated variability in inter-sensor biases. The objective is to characterize any possible temporal or spatial variability, identify the underlying dependencies that affect radiometer data, differentiate

Instrument Pair	Oscillation Period from Model (day)	Oscillation Period from Observation (day)	Maximum Magnitude of GMI/TMI TB Oscillation (K)	Maximum Magnitude of DD Oscillation(K)
GMI/AMSR2	40	41	61@89H	1.5@89H
GMI/SSMIS (F16)	40	41	58@89H	1.6@89H
GMI/SSMIS (F17)	40	41	64@89H	1.7@89H
GMI/SSMIS (F18)	40	41	62@89H	1.7@89H
GMI/TMI	52	56	49@89H	1.8@89H
GMI/WindSat	40	41	62@23.8V	1.9@23.8V
TMI/WindSat	24	23	53@21V	2.1@21V
TMI/AMSR2	24	24	54@85.5H	2@85.5H
TMI/SSMIS (F16)	24	24	52@85.5H	2@85.5H
TMI/SSMIS (F17)	24	24	55@85.5H	2.1@85.5H
TMI/SSMIS (F18)	24	24	53@85.5H	2@85.5H

Table 1. Oscillation periods (orbital model and observation) and maximum magnitudes (GMI/TMI) in inter-sensor biases. For instance, when comparing GMI/AMSR2, the maximum oscillation is found at channel 89H with magnitudes of 61 and 1.5 K for TB and DD respectively.

Return to Page 1

simulation and instrument errors, and reduce inter-sensor biases in future inter-calibration effort. The data are from Global Precipitation Measurement (GPM) mission including a total of 7 constellation radiometers and 11 pairing combinations. Inter-sensor biases are calculated based on collocating the field of view (FOV) of different radiometers over the ocean. A radiative transfer model (RTM) is used with ancillary reanalysis data to simulate brightness temperatures (TBs) and account for instrument differences in frequency, Earth incidence angle (EIA), and bandwidth. The single difference (SD) is defined as the difference of observed minus simulated TB for an individual radiometer, while the double difference (DD) is the difference of the SD of the target radiometer minus that of the reference radiometer. DD represents the inter-sensor biases. Comparing SD and DD gives a sense of the magnitude of simulation biases and actual radiometer calibration biases. A ubiquitous periodic variation in radiometer inter-sensor biases is found. The power spectra of inter-sensor difference time series show a clear signal with ~40 day period in both SD and DD. This 40 day signal is present in all channels. Table 1 shows the oscillation periods of different radiometer pairs. The oscillation is significant with a maximum magnitude of 4 K and 2 K for SD and DD, respectively. It is worth noting that the 40-day oscillation is also present in direct inter-sensor biases (TBs of target minus reference radiometers) without model simulation. This further indicates the ubiquitous presence of inter-sensor bias variability, as it is not affected by model simulation. The oscillation is correlated to the change of collocation geographic regions which is determined by the spacecraft orbits. The latitude of the collocations changes periodically between high latitudes and the tropics and appears as the superposition of two sinusoidal waves symmetric about the equator. Figure 1 show the latitudinal variability for SD and DD (GMI/WindSat), respectively. The Fourier transform is implemented and indicates that the period of oscillation is ~40 days as same as that of the SD and DD. In addition, a pronounced latitudinal dependence is noted. The red and blue ellipses highlight the positive and negative departures, respectively. A high single difference is observed in the tropics for channels 10.65H, 18.7H, and 23.8V, whereas smaller double differences are present in tropics for channels 18.7H and 23.8V.

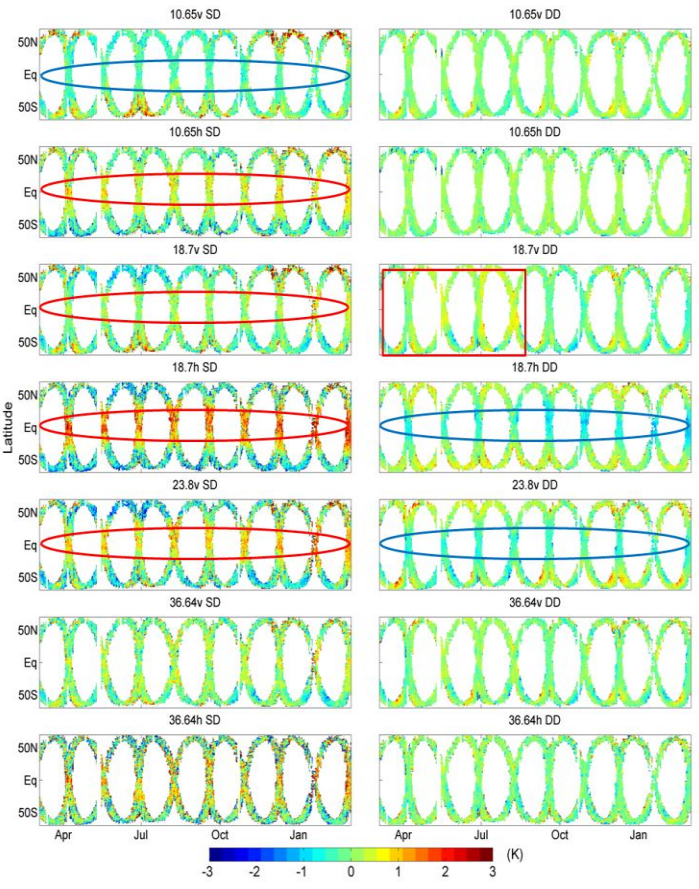

Figure 1. The temporal variability of latitude dependent single (GMI) and double difference (GMI/WindSat) with highlighted positive or negative departures. It has the same 40-day periodicity as single and double differences.

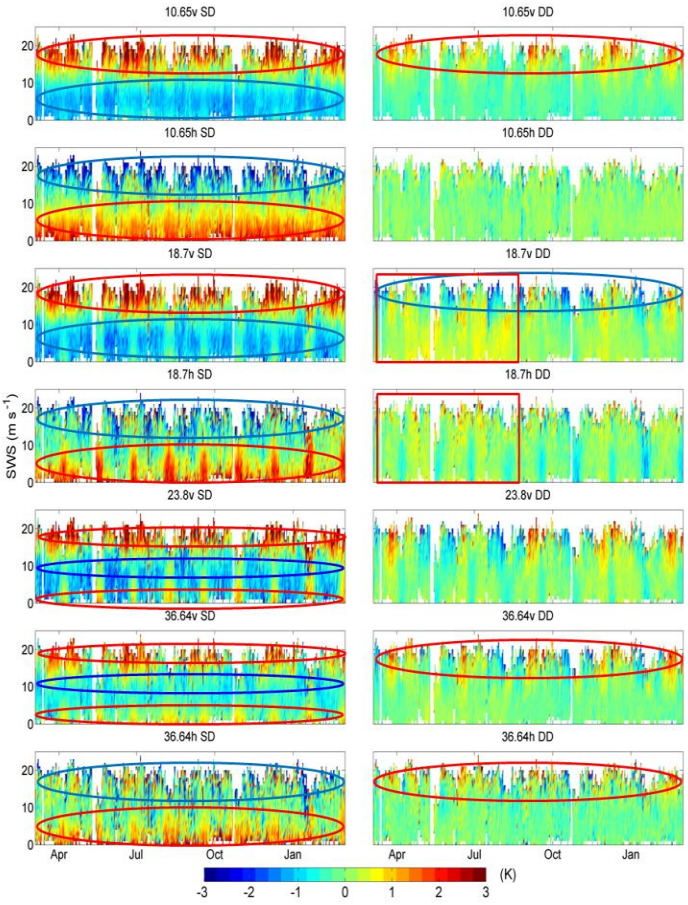

Figure 2. The impact of surface wind speed on single (GMI) and double difference (GMI/WindSat). Both monotonic and non-monotonic features are present.

Return to Page 1

An analytical orbit model is developed. It accounts for spacecraft orbit precession and explains the oscillation period (Yang et al., 2016):

$$T = \frac{360}{2\times 6.529\times 10^{24}\left|a_1^{-3.5}\cos i_1 - a_2^{-3.5}\cos i_2\right|}$$

where T is the oscillation period in units of days, a is the semi-major axis of the spacecraft orbit (the summation of the Earth radius and the spacecraft altitude), i is the orbit inclination angle. The analytic model agrees well with observations as shown in Table1.

Figure 2 shows the impact of surface wind speed (SWS) on single and double differences (GMI/WindSat). Both monotonic and non-monotonic dependences are found at different channels. For 10.65H, 18.7H and 36.64H, SD monotonically increases with SWS; it decreases for 10.65V, 18.7V, 23.8V, 36.64V. Non-monotonic dependence is noticed for 23.8V and 36.64V, where large SD is observed with both very low (<5 m/s) and high (>15 m/s) SWS. The DD becomes either very large (10.65V, 18.7H, 23.8V, 36.64V, 36.64H) or very small (18.7V) with SWS larger than 15 m/s. Inter-sensor biases are found to be dependent on geophysical parameters. The standard deviations for SD and DD are found to be as large as 3.7 and 2.9 K respectively, and they have complex temporal and spatial patterns which cannot be removed by simple linear regression.

Inter-sensor biases show temporal and regional variability and non-monotonic dependence on geophysical parameters. Different patterns in variability can relate to errors in instrument and RTM simulations. In particular, the impact of different RTMs and ancillary geophysical data appears significant and should be further investigated. Differences in reanalysis data have been noted to bias the simulations. RTMs including surface emissivity models and atmospheric absorption models are generally empirically parameterized. Errors due to inaccurate parameterization can result in discrepancies in inter-sensor biases as found here. A comprehensive comparison between different RTMs, ancillary data (reanalysis data, radiosonde and GPS occultation) can help quantify uncertainties with simulations.

Reference

Yang, J. X., D. S. McKague, and C. S. Ruf (2016), Uncertainties in radiometer intercalibration associated with variability in geophysical parameters, Journal of Geophysical Research: Atmospheres, 121(19), 2016JD024937, doi:10.1002/2016JD024937

Discuss the Article

News in this Quarter

Geostationary Operational Environmental Satellite R-Series (GOES-R) launched

by Xiangqian Wu, NOAA

Geostationary Operational Environmental Satellite R-Series (GOES-R) for the National Oceanic and Atmospheric Administration (NOAA), was launched by the National Aeronautics and Space Administration (NASA) aboard a United Launch Alliance (ULA) Atlas V rocket on November 19, 2016 at 1142 UTC (6:42 p.m. EST) from Cape Canaveral Air Force Station in Florida, USA. After a number of orbit lifting manœuvres, it reached the geostationary orbit on November 29, 2016, and officially became GOES-16. The launch is a complete success. This is the first of four satellites in the R series that will support NOAA's geostationary constellation through 2036. The primary payload of GOES-R is the Advanced Baseline Imager (ABI) that has two visible channels, four near infrared channels, and ten thermal infrared channels that monitor the Earth's land, ocean, atmosphere, and ecosystem. Nominally, ABI provides every 15 minutes one image of the entire earth that is visible from its advantage point (full disk or FD), three images that comfortably cover the continental United States (CONUS), and 30 images of mesoscale weather systems (MESO). Alternatively ABI can scan the Full Disk (FD) in five minutes. It has been well known that, compared to the Imager onboard the current GOES I-Series, ABI has roughly three times more channels (from 5 to16), four times better spatial resolution (from 1 km and 4 km for visible and IR channels, respectively, to 0.5 km and 2 km), and five times faster refresh rate (from 26 minutes to 5 minutes). Not as well known (Fig 1) is that the ABI channels have been optimized in terms of spectral response functions (SRF) that often match the corresponding channels of the Visible Infrared Imaging Radiometer (VIIRS) and Moderate-resolution Imaging Spectroradiometer (MODIS).

Figure 1: GOES-R in comparison with its predecessors. (Image Curtsy NOAA)

This makes these channels not only suitable for quantitative applications but also easier for inter-calibration. Additionally, ABI data are expected to have much improved quality including radiometric calibration (bias, dynamic range, and noise, thanks in part to the increased bit depth), imaging fidelity (Modulation Transfer Function or MTF), and image navigation and registration (INR) accuracy. The GOES-R Calibration Working Group (CWG) has been working closely with colleagues at the Japan Meteorological Agency (JMA) in the past five years under a bi-lateral agreement to exchange information related to NOAA's GOES-R and JMA's Himawari programs. This cooperation was initiated within the GSICS framework and has benefited GOES-R in many aspects.

The other Earth-viewing instrument onboard GOES-R is the Geostationary Lightning Mapper (GLM), the first of its kind in geostationary orbit. GLM monitors lightning (cloud-to-ground, cloud-to-cloud, and in-cloud) 500 times every second at the nominal and nearly uniform spatial resolution of 10 km that covers up to 52° away from nadir. It senses the characteristic lightning signal at 777.4 nm to detect lightning day and night. It is exciting to monitor lightning side by side with ABI; a lot can be learned from this combination than either instrument alone, for both instruments and for the phenomena being monitored. GLM shares some common calibration techniques with ABI such as vicarious calibration using deep convective clouds (DCC).

In addition to Earth-viewing, space weather monitoring is another important part of the GOES-R mission. This will be accomplished with four space sensors and the required ground segment. The Magnetometer (MAG) measures *in situ* three components of the geomagnetic field. The Space Environment In-Situ Suite (SEISS) is composed of four sensors to monitor heavy ion fluxes, low energy protons and electrons, high energy protons and electrons, and solar and galactic protons. The Solar Ultraviolet Imager (SUVI) images the Sun in six bands ranging from 94 nm to 304 nm. And the Extreme Ultraviolet and X-Ray Irradiance Sensors (EXIS) monitor solar irradiance at very short wavelength.

Furthermore, beyond the earth and space weather monitoring, GOES-R continues its contributions to the Search and Rescue Satellite Aided Tracking (SARSAT) System, an international satellite-based search and rescue network operated by NOAA. GOES-R carries a special transponder that can detect distress signals from emergency beacons.

GOES-16 arrived at its test station (89.5W) on December 5, 2016. Outgassing continues for most instruments at writing time. Post-Launch Testing (PLT) will start shortly to verify instrument functioning. Successful PLT is expected to lead to Beta Maturity, which will trigger the start of Post-Launch Product Testing (PLPT). CWG will lead PLPT to verify the quality of instrument products (Level 1b or L1b). Completion of the PLPT would also lead to the ABI L1b products achieving Provisional Maturity. After a thorough characterization of the ABI performance GOES-R would be handed over to NOAA operation.

The NOAA's GSICS Processing and Research Center (GPRC) personnel and GOES-R CWG members Xiangqian Wu, Bob Iacovazzi, and Fangfang Yu had the honor to witness the launch. While the launch was flawless, the hours before the launch were tense and dramatic. Unexpected technical and procedural events delayed the launch repeatedly, and it came down to the

Return to Page 1

final chance, the last minute of the one-hour launch window. We were no longer entertained by alligators floating in front of us, and the evening chill crept in after sunset. Then all anomalies were cleared miraculously, the 20+ systems all responded to the Final Poll with "GO", "CLEAR", "PROCEED", and finally "Launch Director is GO, and you have the permission to launch". Loud cheers arose from the crowd after that. The launch was spectacular, though mostly silent, until "Mach 1" (the rocket broke the sound barrier) was announced and, several seconds later, we heard and felt the acoustic boom. That was as memorable as the scene. Discuss the Article

Outcomes of the GSICS Users Workshop 2016

by Manik Bali, Lawrence E Flynn, Xiangqian Wu, Ralph Ferraro, NOAA, Dave Doelling(NASA) , Tim Hewison(EUMETSAT) and Masaya Takahashi(JMA)

The GSICS Coordination Center (GCC) organized the 2016 GSICS Users Workshop (GUW) at the NOAA Center for Weather and Climate Prediction (NCWCP), College Park, MD, USA on 11 Aug 2016. It was concurrent with the Annual NOAA Joint Polar Satellite System (JPSS) Science Meeting.

Taking into account increased interest in GSICS activities in the satellite community in recent years, for the first time the GUW was expanded to an entire day. The GUW consisted of four sessions each of 1.5 Hr and brought together a wide audience of GSICS product planners, creators and product users. Each session was roughly dedicated to an individual GSICS subgroup (IR, MW, VIS or UV). Over 60 members participated in the GUW.

A key aim of the GUW was to introduce the NOAA Integrated Calibration Validation System (ICVS) to the GSICS Community. The ICVS is emerging as a key tool developed under the JPSS program that reveal real time information of satellite health. It is envisaged that integration of the ICVS into the GSICS satellite monitoring can help in detection and root cause analysis of anomalies in instrument measurements during the lifetime of the instruments.

The GCC Director Larry Flynn and Deputy Director Manik Bali Co-chaired the workshop. The workshop and GSICS were introduced by Mitch Goldberg, JPSS Program Scientist and former Chair of the GSICS Executive Panel. This was followed by an overview of the past year's GSICS activities by Ken Holmlund (GSICS EP Vice Chair).

On behalf of GSICS Research Working Group (GRWG) Chair Dohyeong Kim and GRWG Vice Chair Tim Hewison, Fred Wu presented an overview of the GRWG, including its structure, membership, and typical activities. This was followed by examples of current projects for each subgroup giving a sense of the depth and variety of GRWG interests. The selected activities were: pioneering attainment of a GEO ring for calibration in the infrared (IR) subgroup; refined calibration methodology and products based on deep convective clouds (DCC) for the visible and near infrared (VNIR) subgroup; SAPHIR-ATMS inter-calibration progress for the microwave (MW) subgroup; and reference solar spectral irradiance comparisons for the ultraviolet (UV) subgroup. It concluded with the identification of two overarching priorities for GRWG, namely interaction with other organizations such as CEOS and the use of primary corrections for climate applications to create homogenized products with transfers to secondary references.

The GCC Director then gave an overview of the GSICS Products and Deliverables, followed by a GSIC Users Survey by the GCC Deputy Director. The survey touched upon requirements from users of the GSICS Products that were collected over the last one year. The survey has confirmed the GSICS resolve to produce user-driven deliverables in the future. Following are summaries for each session.

ICVS (Integrated Calibration Validation System)

The ICVS was described in four talks. The first one, by F. Weng, described the performance of the JPSS instruments (ATMS, CrIS VIIRS and OMPS) and discussed their suitability for use as in-orbit GSICS references. The second talk, by L. Brown, described the organization, design and content of the ICVS as a web-based monitoring system. The third talk, by T. Choi, was on the scientific content of the ICVS monitoring. The fourth talk, by N. Sun, was on a central function of the ICVS, namely, system alerts and other notifications which are immensely helpful in diagnosing problems.

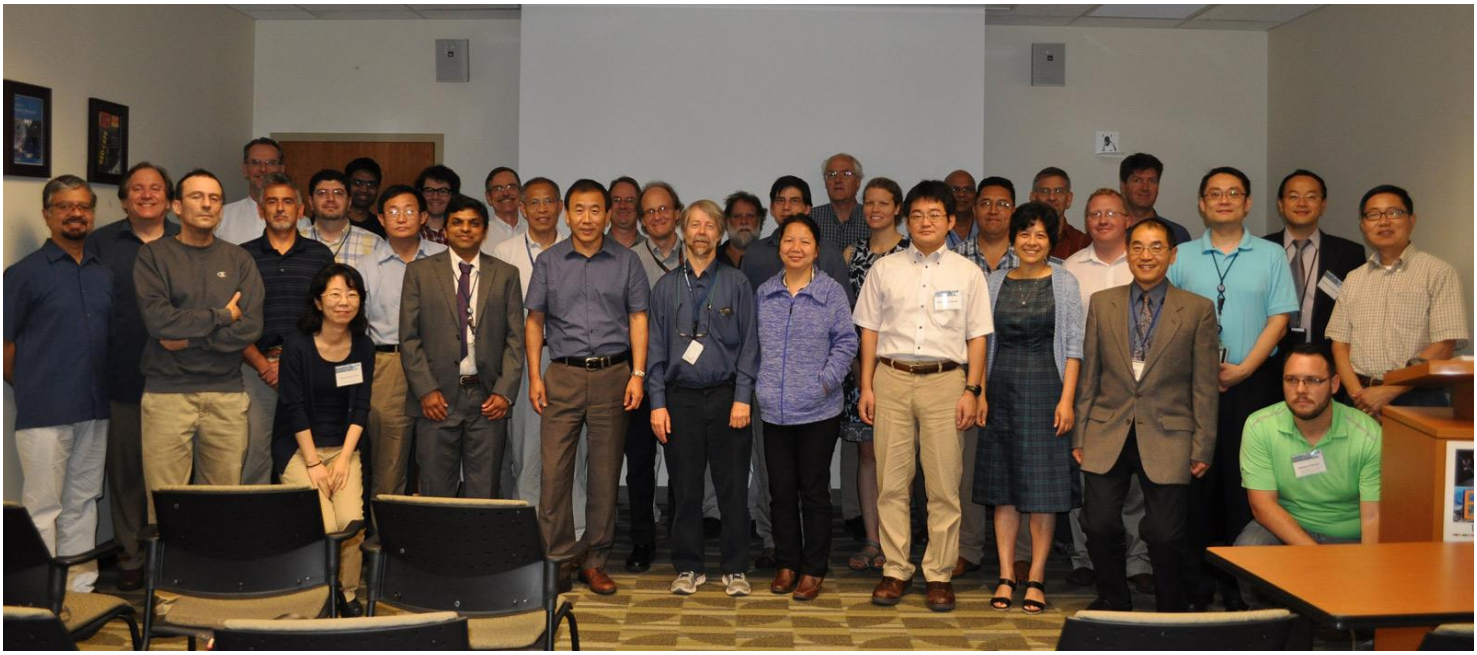

Some of the participants of the GSICS Users Workshop 2016

Microwave Session (Chair Ralph Ferraro)

Four different users of MW products and tools were selected as speakers for the session in order to get a broad perspective of their needs from GSICS. The first speaker, Wes Berg from Colorado State University (CSU) and the chair of the NASA Global Precipitation Measurement (GPM) Cross-Calibration (XCAL) Team, focused on the uncertainties in microwave radiative transfer, stressing the need to improve surface emissivity and water vapor absorption models. He recommended using high quality in-situ data like ocean buoys and GRUAN radiosondes instead of NWP model fields. Also, the X-CAL group advised that both the GMI and MHS sensors could serve as good references.

The second speaker, John Forsythe, also from CSU, is the creator of a MW blended water vapor product (both Total Precipitable Water – TPW and layered PW) that requires accurate calibration for use on both weather and climate scales. Using a L1C type of climate data record would help develop a vastly improved TPW climatology. He also stressed the importance of "image validation" to confirm the validity of the MW L1 data used to generate the water vapor products.

The final two speakers of the session were climate product developers. George Huffman, deputy project scientist for GPM from NASA/Goddard Space Center, spoke about the Global Precipitation Climatology Project (GPCP) 30-year merged MW and IR satellite product. These data require stable, long term corrections to the input sources on the order of 1 K. A unified parallax correction from GSICS would be desirable for the GEO IR data. Lastly, Cheng-Zhi Zou from NOAA/NESDIS provided a status of the long-terms MW time series for atmospheric temperature monitoring from the SSU/MSU through AMSU (and eventually expanding to include ATMS). A wide variety of methods are used to perform sensor calibration and inter-satellite calibration.

The discussions in the session lead to an open question as to how to detect and mitigate impacts of frequency shifts. A key step of this would involve RTM Vs Satellite inter-comparisons. This lead to a recommendation **Recommendation:** GSICS-led RTM inter-comparison study for specific components like emissivity and WV absorption.

IR Session (Chair Fred Wu)

F. Wu provided an overview of algorithm, products, and planned development of GSICS inter-calibration for IR using hyperspectral sounders. M. Takahashi described recent work of Advanced Himawari Imager (AHI) inter-calibration using Cross-track Infrared Sounder (CrIS) as reference. P. Thapliyal introduced remotely the GSICS activities for inter-calibration of the INSAT-3D radiance at Indian Space Research Organization (ISRO). A. Harris, a developer of sea surface temperature (SST) products, presented requirements for GSICS from a user's perspective. It was felt that GSICS Correction, developed to homogenize satellite observations, are also powerful tools to characterize, diagnose, and improve satellite instrument calibration. Experienced users can further help with this

Return to Page 1

endeavor.
Recommendation: It is highly desirable to share the GSICS intermediate dataset and products with users.
VIS Session (Chair Dave Doelling)

Andy Heidinger presented a new global all-sky VIS/NIR reflectance method to calibrate AVHRR data. After correcting for orbital drift using theN18 model, the VIS/NIR global all-sky reflectance gave similar results to the PATMOS-X calibration. He validated the method for Aqua-MODIS band 1 and saw a -1% drift over the 15 years. *It might be worthy of a GSICS VIS/NIR standard method since it can be used for all visible sensors.*
Matthijs Krijger presented lunar SCIAMACHY hyper-spectral irradiances that were characterized according to phase angle and ASM angle after accounting for instrument degradation. The SCIAMACHY team also participates in the GIRO project. *NASA-Langley and the SCIAMACHY team will keep in touch to update the NASA SBAF tool with the latest SCIAMACHY version when it becomes available to improve the SBAF tool. Dave also mentioned that his group received NASA ROSES funding to expand the SBAF tool.*
Grant Matthews presented a SI traceable lunar observation mission, the Moon and Earth Radiation Budget Experiment (MERBE). Jack Xiong presented the latest MODIS and VIIRS onboard calibration details.

Dave Doelling presented the goals of the GSICS VIS/NIR sub-group. *Fred Wu noted that all of the Meteosat-10 vicarious calibration methods had the same seasonal cycle and asked if it might be sensor related.*
UV (Chair Larry Flynn)

The workshop concluded with a discussion of UV projects on comparison of solar measurements, UV reflectivity and ozone profiles initiated in the UV subgroup. The projects now have participation by researchers working on OMI, GOME-2, SCIAMACHY, and OMPS measurements. CMA will have a visiting researcher at the UMD CICS next year working with NOAA researchers on UV measurements. This work will be a link to expand the UV projects to future CMA hyperspectral UV instruments.
Further details on the meeting and author presentations can be accessed on the wiki page at http://gsics.atmos.umd.edu/bin/view/Development/UsersWorkshop2016

Discuss the Article

Announcements

2017 GSICS Annual Meetingto be held in Wisconsin, Madison, USA, March 20-24, 2017

by Doheyong Kim (KMA), Masaya Takahashi (JMA) and Manik Bali,(NOAA)

The 2017 GSICS Annual meeting will be held 20-24 March 2017 at the Pyle Center of University of Wisconsin-Madison. It would be hosted by the National Oceanic and Atmospheric Administration (NOAA) and the University of Wisconsin Cooperative Institute for Meteorological Satellite Studies (CIMSS).

A meeting page has been created on the GSICS wiki at http://gsics.atmos.umd.edu/bin/view/Development/20170320. Topics likely to be covered and final presentations would be posted on this page. Following precedent the 2017 annual meeting would have three main sessions. It would begin with a Mini Conference-that would discuss items to introduce GSICS products and deliverables that are not yet directly linked to GSICS Products. This will be followed by a Plenary Session following which the GSICS Data Working Group (GDWG) and the GSICS Research Working Group (GRWG) will break out into parallel sessions while converging on important topics. The meeting will finish with a wrap up session where a summary of the meeting and the status of action items will be discussed.
An optional no-host dinner is planned at the cost of $35. For registration and details of the meeting visit
http://www.ssec.wisc.edu/meetings/gsics/
For additional information on the venue or program, please contact Andy Heidinger (Andrew.Heidinger (AT) noaa.gov) or the GRWG Chair Doheyong Kim (dkim (AT) kma.go.kr) or the GDWG Co-Chair (Masaya Takahashi (m_takahashi(AT) met.kishou.go.jp) .

SPIE Optics and Photonics Earth Observing Systems XXII conference to be held in San Diego Aug 6-10, 2017

by James Butler, NASA
The annual SPIE Optics and Photonics' Earth Observing Systems XXII conference will be held August 6-10, 2017 at the San Diego

Convention Center, San Diego, CA.

The Earth Observing Systems XXII conference welcomes the submission of papers over a wide range of remote sensing topics. Papers are being solicited in the following general areas:

- on-orbit and planned Earth-observing missions including new system requirements and plans
- commercial system designs
- electro-optical sensor designs and sensitivity studies
- ultraviolet through thermal infrared, microwave, radar, and lidar remote sensing systems
- CubeSat and NanoSat instruments and technologies
- instrument sub-system and system level pre-launch and on-orbit calibration and characterization
- vicarious calibration techniques and results
- satellite instrument airborne simulators
- techniques and approaches in remote sensing data processing, reprocessing, archival, dissemination, and utilization
- conversion from research to operational systems
- pre-launch and on-orbit instrument calibration, performance, and characterization
- on-orbit instrument inter-comparison techniques and results
- enabling technologies (optics, antennas, electronics, calibration techniques, detectors, and models)
- sensor calibration traceability, uncertainty, and pre-launch to on-orbit performance assessments.

The conference call for papers is available online at http://spie.org/OP405. Conference abstracts are due 23 January 2017**,** and proceedings manuscripts are due 10 July 2017.

The Characterization and Radiometric Calibration for Remote Sensing (CALCON) Annual Meeting will be held August 21–24, 2017 at Utah State University, Logan, UT

By James Butler, NASA

Now in its 26th year, the Characterization and Radiometric Calibration for Remote Sensing (CALCON) Annual Meeting provides a forum for scientists, engineers, and managers to present, discuss, and learn about calibration, characterization, and radiometric issues within the microwave, IR, visible, and UV spectral ranges. Individuals developing measurement requirements for current and future sensor systems are encouraged to participate in the meetings to foster continuity and advancement within the community. CALCON attendance promotes interaction with other experts and helps close the gap between expectations and real-world experiences. Collaboration often results in the discovery of solutions to individual program challenges.

Conference information is available at www.calcon.sdl.usu.edu. The deadline for the Call for Papers is 4 April 2017with the website open for abstract submittal in January 2017.

GSICS-Related Publications

Barrientos, C., Mattar, C.,Nakos, T., W. Perez.,2016, Radiometric Cross-Calibration of the Chilean Satellite FASat-C Using RapidEye and EO-1 Hyperion Data and a Simultaneous Nadir Overpass Approach. Remote Sens. *8*, 612. doi:10.3390/rs8070612

Bhatt, R., Doelling, D. R., Scarino, B. R., Gopalan, A., Haney, C. O., Minnis, P and K. M. Bedka., 2016, A consistent AVHRR visible calibration record based on multiple methods applicable for the NOAA degrading orbits. Part I: Methodology. J. Atmos. Oceanic Technol., 33, 2499–2515. doi: 10.1175/JTECH-D-16-0044.1

Berg, W., Bilanow, S., Chen, R., Datta, S., Draper, D., Ebrahimi, H., Farrar, S., Jones, W.L., Kroodsma, R., McKague, D.,Payne, V., Wang, J., Wilheit, T. and Yang, J. X., 2016, Intercalibration of the GPM Microwave Radiometer Constellation. *Journal of Atmospheric and Oceanic Technology*, (2016). doi: *10.1175/JTECH-D-16-0100.1*

Chang, T., Xiong ,X., Q. Mu.,2016, VIIRS Reflective Solar Band Radiometric and Stability Evaluation Using Deep Convective Clouds. IEEE Transactions on Geoscience and Remote Sensing.,99, 1-9, doi: 10.1109/TGRS.2016.2594029

Doelling, D.R., Haney, C.O., Scarino, B.R., Gopalan, A. and Bhatt, R., 2016. Improvements to the Geostationary Visible Imager Ray-Matching Calibration Algorithm for CERES Edition 4. Journal of Atmospheric and Oceanic Technology, *33*(12), pp.2679-2698.doi: 10.1175/JTECH-D-16-0113.1

Jiang, G. M., Wang, Z. Y and J. Wang., 2016, Inter-Calibration of VIRR/FY-3A/B Split-Window Channels with AIRS/Aqua and IASI/Metop-A Measurements'. International Journal of Remote Sensing 37 (22): 5249–69. doi:10.1080/01431161.2016.1232873.

Scarino, A. Gopalan, C. O. Haney, P. Minnis, and K. M. Bedka, 2016: A consistent AVHRR visible calibration record based on multiple methods applicable for the NOAA degrading orbits, Part II: Validation. J. Atmos. and Oceanic. Tech, In Press. doi: 10.1175/JTECH-D-16-0042.1

Siliuk, O. O and L.V. Katkovskii., 2016., Methods and Results of Image Cross-Calibration of the Belarusian Satellite and Other Sensors. Sovremennye Problemy Distantsionnogo Zondirovaniya Zemli Iz Kosmosa, 13 (4): 261–70. doi:10.21046/2070-7401-2016-13-4-261-270.

Min, M., Cao, G., Xu, N., Bai, Y., Jiang, S., Hu, X., Dong, L., Guo, J., P. Zhang.,2016, On-Orbit Spatial Quality Evaluation and Image Restoration of FengYun-3C/MERSI. IEEE Trans. Geoscience and Remote Sensing 54(12): 6847-6858 (2016) doi: 10.1109/TGRS.2016.2569038

Peng, G., Shi, L., Stegall, S.T., Matthews, J.L. and Fairall, C.W., 2016. An evaluation of HIRS near-surface air temperature product in the Arctic with SHEBA data. Journal of Atmospheric and Oceanic Technology, 33(3), pp.453-460.

Yang, J., 2016. Spaceborne Microwave Radiometry: Calibration, Inter-calibration, and Science Applications. PhD Thesis, University of Michigan.

Zou, X., X. Zhuge, and F. Weng, 2016, Characterization of bias of advanced Himawari imager infrared observations from NWP background simulations using CRTM and RTTOV. J. Atmos. Oceanic Technol., 33, 2553–2567, doi:10.1175/JTECH-D-16-0105.1.

Submitting Articles to GSICS Quarterly Newsletter:

The GSICS Quarterly Press Crew is looking for short articles (~800 to 900 words with one or two key, simple illustrations), especially related to cal/val capabilities and how they have been used to positively impact weather and climate products. Unsolicited articles are received for consideration anytime, and if accepted, will be published in the next available newsletter issue after approval/editing. Note the upcoming spring issue will be a general issue. Please send articles to manik.bali@noaa.gov.

With Help from our friends:

The GSICS Quarterly Editor would like to thank Igor Tomazic for the lead article in this issue. Thanks are also due to Masaya Takahashi, Ralph Ferraro, Xiangqian Wu, Tim Hewison and Manik Bali for reviewing the articles in this issue.